scientific reports

Check for updates

OPEN

The anti-tumor effects of main component (benzethonium chloride) of butorphanol tartrate injection in non-small cell lung cancer

Honglei Tao[1,2,4], Lei Li[1,3,4], Huiling Li[1,4], Tingting Ma[2], Xinping Zhu[2], Jili Cao[2], Yongqiang Zhu[2], Shengmei Zhu[1]✉ & Mingqian Li[2]✉

Cancer is one of the leading causes of morbidity and mortality in the global population. The effective management of cancer-associated pain and anesthesia are critical aspects of comprehensive cancer treatment. However, the role and mechanism of anesthesia and analgesia-related drugs in tumors remain controversial. In this study, the efficacy of 16 commonly used analgesics and anesthetics against non-small cell lung cancer (NSCLC) was evaluated. Among the 16 examined injections, butorphanol tartrate injection significantly inhibited the proliferation of NSCLC cells and increased the sensitivity of the EGFR-TKI-resistant H1975 cell line to gefitinib. Benzethonium chloride (BC) is the main active antitumor ingredient of butorphanol tartrate injection. BC may regulate the cell cycle, apoptosis and EMT signaling pathways by modulating the P53 signaling pathway. Our study reveals the therapeutic value of butorphanol tartrate injection and BC in the treatment of NSCLC and provides a theoretical basis for comprehensive therapies for NSCLC.

Keywords Benzethonium chloride, Butorphanol tartrate injection, P53 signaling pathway, Non-small cell lung cancer

Cancer remains a major global health challenge, causing a significant burden of disease worldwide[1]. Surgery is often the preferred treatment for various types of tumors, including lung cancer, breast cancer, and gastric cancer[2]. Cancer treatment statistics indicate that more than 60% of patients undergo tumor resection[3]. Pain caused by cancer or treatment is unavoidable; therefore, anesthesia and analgesics play important roles in the comprehensive treatment of cancer. Currently, up to 80% of cancer patients receive analgesia and anesthesia management[3].

Non-small cell lung cancer (NSCLC) is one of the leading causes of cancer-related death worldwide[4]. The main treatments for NSCLC are surgery, radiotherapy, chemotherapy, targeted therapy and immunotherapy. Among them, EGFR-TKIs, which target activating mutations in epidermal growth factor receptor (EGFR), have achieved good efficacy, but their application is limited by innate or acquired drug resistance[5]. The main cause of acquired resistance in first- and second-generation EGFR-TKIs is the T790M mutation in exon 20 of EGFR (50%), the main mechanism of which is the substitution of threonine (T) at the 790 site of exon 20 of EGFR for methionine (M), which increases the affinity of ATP for EGFR and competitively hinders the binding of TKIs to EGFR[6]. In addition to the T790M mutation, other mechanisms of acquired resistance include bypass activation (C-Met, HGF and HER2, etc.)[7,8], disruption of the downstream pathway of EGFR (RAS mutation, PTEN deletion, and PIK3Ca mutation, etc.), and histological transformation (non-small cell lung cancer becomes small-cell, and activation of the MET pathway)[9,10]. Therefore, finding or developing drugs to delay or reduce resistance to EGFR-TKIs is the key to improving the efficacy of curative treatment for NSCLC and has become a hotspot for researching NSCLC treatment, which is highly economically and socially important.

[1]Department of Anesthesiology, The First Affiliated Hospital, ZheJiang University School of Medicine, Hangzhou 310009, Zhejiang, China. [2]Zhejiang Academy of Traditional Chinese Medicine, Tongde Hospital of Zhejiang Province, Hangzhou 310012, Zhejiang, China. [3]Affiliated People's Hospital of Ningbo University, Ningbo 315201, Zhejiang, China. [4]Honglei Tao, Lei Li and Huiling Li contributed equally to this work. ✉email: smzhu20088@zju.edu.cn; limingqian613@163.com

Pain caused by lung cancer metastasis or treatment can adversely affect a patient's quality of life and affect the prognosis of the tumor[11]. However, the role of anesthesia and analgesics in tumors is still controversial, so screening for anesthesia and analgesics with antitumor effects in addition to providing clinical analgesia is highly important.

The purpose of this study was to investigate the antitumor effect of analgesic injections on NSCLC and its enhancing effect on EGFR-TKI therapy. We found that butorphanol tartrate injection has a good antitumor effect and that its main anticancer agent is benzethonium chloride (BC), which acts through the P53 signaling pathway, inhibits NSCLC, and enhances sensitivity to EGFR-TKI therapy.

Materials and methods

Cell culture

Four types of NSCLC were used in this study: the lung adenocarcinoma cell lines H1975, A549, and HCC827 and the large cell carcinoma subtype H1299. Among them, the epidermal growth factor receptor-TKI-resistant cell line H1975 contains the L858R-activating mutation and the epidermal growth factor receptor T790M-resistant mutation. The HCC827 cell line has an EGFR-activating mutation (E746-A750 deletion mutation).

The H1975 and A549 lung cancer cell lines were procured from the Institute of Biochemistry and Cell Biology, Chinese Academy of Sciences, while the H1299 and HCC827 cell lines were obtained from Procell (Wuhan, China). The cells were cultured in complete RPMI 1640 medium, which consisted of 10% fetal bovine serum and 1% penicillin/streptomycin (ExCell Bio, China), in a humidified incubator at 37 °C with 5% CO_2.

Cell viability assay

The H1975, A549, H1299, and HCC827 cell lines were seeded into 96-well culture plates at a density of 3×10^3 cells/100 µl per well and incubated overnight in RPMI 1640 medium supplemented with 10% fetal bovine serum. Following cell adhesion, drugs were added at various concentrations. H1975, A549, H1299, and HCC827 cells were treated with 16 anesthetic and analgesic drugs (40 µg/ml) for 72 h. H1975, A549, H1299, and HCC827 cells were treated for different durations (24, 48, and 72 h) at various doses (0, 5, 10, 20, 40, 60, and 80 µg/ml). H1975 cells were treated with different concentrations of butorphanol tartrate and benzethonium chloride (0–80 µg/ml) for 24, 48, and 72 h. H1975 cells were treated with different concentrations of benzethonium chloride (0–20 µM) for 24, 48, and 72 h. Equal amounts of gefitinib and benzethonium chloride (0, 2.5, 5, 10, 15, or 20 µM of each) were coadministered to H1975 cells for 24 h. H1975 cells were treated with 10 µM gefitinib and benzethonium chloride (0, 1, 2, 4, 6, 8, 10, 15, or 20 µM) for 24, 48, or 72 h.

After incubation with the drugs for 24, 48, or 72 h, 10 µL of CCK8 reagent (ApexBio, China) was added to each well, and the mixture was incubated for an additional 1–2 h. The plates were then shaken for 2 min, and the absorbance at 450 nm was measured using a SpectraMax i3 (Molecular Devices, USA). Dose–response curves were generated via GraphPad Prism software (version 8.3.0, https://www.jb51.net/softs/702273.html), and hal f-maximal inhibitory concentrations (IC_{50}) were calculated for NSCLC cells.

Cell colony formation assay

The cells (500–1000) were added to each well of a six-well plate, maintained in triplicate. H1975, A549, H1299 and HCC827 cells were treated with different concentrations (0, 5, 10, or 20 µg/ml) of butorphanol tartrate injection. H1975 cells were treated with different concentrations (0, 2, 5, or 8 µM) of benzethonium chloride. The cells were incubated at 37 °C for a period of 6–7 days until they adhered to the surface of the plate. The cells were subsequently treated with various concentrations of drugs and maintained at 37 °C for an additional 6–7 days. Following treatment, the cells were fixed with methanol for 15 min and stained with crystal violet (Beyotime, China) for 20 min. The colony formation rate was determined by calculating the number of colonies formed using ImageJ software (version 1.8.0, https://www.6z6z.com/rj/7595.html).

Cell cycle and apoptosis detection

The H1975 cells were seeded into 6-well plates and allowed to adhere for 24 h before treatment with benzethonium chloride (BC), gefitinib, or a combination of both. In this group, the BC drug concentrations were 0, 2, 5, and 8 µM in the alone group, and the control wells were treated with an equal amount of DMSO for 24 h. The BC combined with gefitinib group was treated with a fixed concentration of 10 µM gefitinib and BC (0, 2, 5, and 10 µM) for 24 h. Following treatment, the cells were washed with precooled PBS and then collected by centrifugation at 800 rpm for 5 min. The collected cells were fixed with 70% ethanol (prepared in deionized water) for 6 h and then centrifuged at 1500 rpm for 5 min to remove the ethanol. The cells were subsequently washed three times with precooled PBS and stained with 400 µL of propidium iodide (PI) dye, after which they were transferred to a flow tube. The cells were then incubated at room temperature in the dark for 15 min, and changes in the cell cycle were analyzed via flow cytometry. Modfit software (version 5.0, https://www.vsh.com/products/mflt/index.asp) was used to calculate the results and determine the percentage of cells in each phase of the cell cycle.

The H1975 cells were cultured in 6-well plates for 24 h and subsequently subjected to various treatments, including benzethonium chloride, gefitinib, and a combination of both compounds. In this group, the BC drug concentrations were 0, 2, 5, and 8 µM in the alone group, and the control wells were treated with an equal amount of DMSO for 24 h and 48 h. The BC combined with gefitinib group had a fixed concentration of 10 µM gefitinib and BC (0, 2, 5, and 10 µM) for 24 h of H1975 cell treatment. The apoptosis rates of both untreated and treated cells were determined via an Annexin V-FITC apoptosis detection kit. Harvested cells, both floating and adherent, were washed three times with phosphate-buffered saline (PBS) and stained with Annexin V and propidium iodide (PI) in binding buffer (Procell, China) for 30 min in the dark. Apoptosis was detected using a FACSCalibur flow cytometer (BD Biosciences, USA) with an acquisition threshold of 10,000 events per sample.

The obtained data were analyzed using FlowJo software (version 7.6.1, https://soft.3dmgame.com/down/251874.html) to determine the percentage of apoptotic cells.

RNA isolation and quantitative real-time PCR

Total RNA was extracted using TRIzol reagent (Haoke, China), and its quality and quantity were assessed via a Nanodrop One instrument (Thermo Fisher Scientific, USA). Subsequently, 1 μg of total RNA was subjected to reverse transcription using the PrimeScript RT reagent Kit with gDNA Eraser (Novogene, China) according to the manufacturer's instructions. Quantitative real-time PCR was performed using TB Green Fast qPCR mix (Yugong Biotech, China) following the manufacturer's protocol, with all of the reactions performed in triplicate. The resulting data were normalized to the level of expression of the housekeeping gene GAPDH.

Western blot analysis

The cell or tumor tissue samples were homogenized in protein lysis buffer supplemented with protease and phosphatase inhibitor cocktail (Boster, China). The resulting homogenates were subjected to centrifugation at 12,000 rpm for 10 min at 4 °C, and the resulting debris was removed. The protein concentrations of the resulting supernatants were determined via a modified BCA detection kit (Sangon Biotech, China). The protein samples were subsequently mixed with loading buffer and electrophoresed on 8%-12% SDS-PAGE gels. The proteins were then transferred to PVDF membranes (Bio-Rad), which were blocked with 5% skim milk in TBST for 1.5 h at room temperature. The membranes were then incubated overnight at 4 °C with the indicated primary antibodies. Following three washes with TBST, the membranes were incubated with secondary antibodies for 1 h. Finally, the immunoreactive bands were visualized via an enhanced chemiluminescence (ECL) kit (Haoke, China).

Tumor cell migration assay

The wound healing test plug-ins (IBIDI, Germany) were subjected to 10 min of soaking in a 75% ethanol solution, followed by UV light irradiation for 1 h. H1975 cells were seeded in six-well plates equipped with wound healing test inserts at a concentration of 4×10/well. The cells were then starved for 24 h in serum-free medium before the removal of the test inserts and the addition of fresh medium containing varying concentrations of benzethonium chloride and gefitinib. The dosing time was taken as 0 h, and images were captured at 0 and 24 h under a microscope. The scratch area was calculated using ImageJ software (version 1.8.0 https://www.6z6z.com/rj/7595.html).

To evaluate invasion and migration, 24-well Transwell inserts were utilized, some of which were coated with Matrigel (BD Biosciences, USA). The inserts were fixed with 0.4% paraformaldehyde and stained with 0.1% crystal violet. Three to five randomly selected fields were imaged and counted using ImageJ software (version 1.8.0 https://www.6z6z.com/rj/7595.html).

Transcriptomic analysis

H1975 cells were seeded in a six-well plate at a density of 5×10^5 cells/well. Following overnight cultivation, the cells were treated with 10 μM benzethonium chloride for 24 h, after which they were extracted via the TRIzol method. Transcriptome sequencing of the extracted samples was carried out by Novogene. Differential gene expression analysis was performed via DESeq2 package (version 1.38.3, https://github.com/thelovelab/DESeq2). The clusterProfiler package (version 4.6.2) was used to perform gene set enrichment analysis (GSEA) to identify enriched functional categories. The enrichment pathways of these differential genes were determined using Kyoto Encyclopedia of Genes and Genomes (KEGG) analyse[12–14].

In vivo antitumor study

All of the animal studies were approved by the Animal Care Ethics Committee of the Zhejiang Academy of Traditional Chinese Medicine and were conducted in compliance with the ARRIVE guidelines. Male BALB/c mice with an average weight of 17–20 g were procured from the Zhejiang Academy of Medical Science. H1975 cells were injected subcutaneously into the left flank of each mouse at a density of 1.5×10^6 cells/100 μL. The BALB/c mice with H1975 xenograft tumors were randomly divided into four groups consisting of six BALB/c mice each, namely, the corn oil model group, benzethonium chloride (20 mg/kg) group, gefitinib (20 mg/kg) group, and benzethonium chloride (20 mg/kg) and gefitinib (20 mg/kg) groups. When the subcutaneous tumors reached approximately 100 mm^3, various concentrations of the drugs were injected intraperitoneally. Tumor size and body weight were monitored every other day for 15 days. The tumor volumes were calculated at specific time points by measuring the length (l) and width (w) and determining the volume ($V = 0.5 \times L \times w^2$). At the end of the treatment, the nude mice were euthanized, and the tumors were excised and weighed.

Hematoxylin and eosin (H&E) staining and immunohistochemistry

Tumors were obtained and subsequently fixed and embedded. The resulting blocks were then sectioned to a thickness of 3–5 μM and subjected to dewaxing procedures. Hematoxylin staining was performed on the sections for 8–15 min, followed by rinsing with 95% ethanol and subsequent eosin staining for a period of 2–5 min. Any remaining liquid was carefully removed from the sections, which were subsequently washed and sealed with water. After being covered with coverslips, the sections were air dried under natural conditions. The immunohistochemical experiments were carried out according to Tan et al.[15]. Immunohistochemical slice scanning was performed using 3D HISTECH.

Statistical analysis

The experimental data were processed using ImageJ (version 1.8.0, https://www.6z6z.com/rj/7595.html) and GraphPad Prism software (version 8.3.0, https://www.jb51.net/softs/702273.html), and statistical analysis was conducted. A t test was used to compare differences between groups, and all of the results are reported as the mean ± SEM. Statistical significance was indicated by $^{*}p < 0.05$, $^{**}p < 0.01$ and $^{***}p < 0.001$, with a P value of less than 0.05 considered significant. All of experiments were performed in triplicate (n = 3), and GraphPad Prism Software (version 8.3.0, https://www.jb51.net/softs/702273.html) was used for all of the statistical analyses. The data are expressed as the means ± SEM, and statistical significance was determined with unpaired t tests unless otherwise indicated. P values < 0.05 were considered statistically significant.

Results

The Effects of clinical anesthetics and analgesics in inhibiting cancer progression and mitigating EGFR-TKI resistance

To investigate whether analgesics and anesthetics have antitumor effects on NSCLC, we screened the effects of 16 anesthetic and analgesic injections (Table 1S) on H1975, A549, H1299 and HCC827 cells via a CCK8 assay. The sixteen injections had different inhibitory effects on cell growth. Butorphanol tartrate injection had the most significant inhibitory effect on cell proliferation (Fig. 1A). EGFR-TKI therapy in lung cancer has achieved remarkable efficacy in patients with EGFR kinase activation mutations, but its inevitable drug resistance is the main reason for its limited clinical use. To address this issue, we assessed the effects of 16 anesthetic analgesic injections in combination with gefitinib on the EGFR-TKI-resistant H1975 cell line. Butorphanol tartrate injection was effective in alleviating H1975 resistance to gefitinib (Figure 1SA). To assess the effects of butorphanol tartrate injection on cellular activity, we performed CCK8 assays on H1975, A549, H1299, and HCC827 cells treated over different time periods (24, 48, and 72 h) at various doses (0, 5, 10, 20, 40, 60, and 80 μg/ml) (Fig. 1B–E and Figure 1SB). Our results revealed that butorphanol tartrate injection inhibited the proliferation of NSCLC cells, and the IC_{50} values of butorphanol tartrate injection were 37.89, 17.76 and 16.09 μg/ml at 24, 48 and 72 h, respectively, for H1975 cells (Fig. 1B and Figure 1SB). We then evaluated the effect of butorphanol tartrate injection on the clonogenic ability of H1975, A549, H1299 and HCC827 cells (Fig. 1F–J).

To identify the effective antitumor components of butorphanol tartrate injection, we analyzed the components of butorphanol tartrate injection via high-performance liquid chromatography (HPLC). The HPLC results revealed that butorphanol tartrate injection was composed of two main peaks, namely, butorphanol tartrate (18 min peak) and BC (39 min peak) (Figure 2SA). To identify the components of the injection that inhibit H1975 cell activity, the effects of butorphanol tartrate and BC on H1975 cell activity were examined via a CCK8 assay. The results showed that butorphanol tartrate did not inhibit the proliferation of H1975 cells after 24, 48, or 72 h of exposure (Fig. 1K). However, BC significantly decreased the cellular activity at a concentration of 10 μg/mL after 24, 48, and 72 h of exposure (Fig. 1L).

BC blocked the cell cycle to inhibit H1975 cell proliferation

BC had a dose- and time-dependent suppressive influence on the proliferation of H1975 cells, with IC_{50} values of 13.25 μM at 24 h, 9.523 μM at 48 h, and 4.985 μM at 72 h (Fig. 2A). The anticancer effects of BC on NSCLC cells were further confirmed via a colony formation assay (Fig. 2B,E). To validate the effect of BC on the cell cycle, H1975 cells were treated with benzethonium chloride for 24 h. BC significantly induced cell cycle arrest in H1975 cells in the G1 phase of the cell cycle (Fig. 2C,F). Flow cytometry was used to investigate the potential of BC to induce apoptosis in H1975 cells via Annexin V-FITC and PI staining after treatment with BC for 24 and 48 h. The findings revealed a marked increase in the percentage of apoptotic cells following 48 h of treatment with BC, with a greater concentration of the compound corresponding to a greater proportion of apoptotic cells (Fig. 2D,G,H). These results showed that BC inhibited the cell cycle and caused H1975 cell apoptosis. In addition, the levels of cell cycle-associated and apoptosis-related proteins were analyzed by immunoblotting. The results showed that benzethonium chloride inhibited the expression of CDK2, CDK4, cyclin D1, and cyclin E2 in H1975 cells (Fig. 2I). Moreover, BC led to a dose-dependent increase in the expression of the proapoptotic proteins BAD and BAX, as well as a concomitant decrease in the levels of the antiapoptotic proteins BCL-2 and BCL-XL, in NSCLC cells (Fig. 2J).

BC inhibits the metastasis of H1975 cells via the EMT signaling pathway

To investigate the effect of BC on the metastasis of H1975 cells, Transwell and wound healing assays were performed. We observed that BC significantly inhibited the migration of H1975 cells after 24 h of treatment, with the inhibitory effect increasing in a concentration-dependent manner (Fig. 3A,D). Similarly, the results of cell invasion assays revealed that the anti-invasive ability of H1975 cells increased with increasing concentrations of BC (Fig. 3B,E). Further verification of the inhibitory effect of BC on H1975 cell metastasis was performed using cellular wound healing assays, which revealed a significant reduction in cell migration ability after treatment with 2, 5, or 8 μM benzethonium chloride for 24 h (Fig. 3C,F). We also confirmed that the protein levels of epithelial–mesenchymal transition (EMT)-related genes, including β-catenin, vimentin, and ZEB1, were significantly downregulated, whereas E-cadherin (E-cad) was upregulated following BC treatment (Fig. 3G).

BC enhanced the sensitivity of EGFR-TKI-resistant cells to gefitinib therapy

Our previous study revealed that butorphanol tartrate injection could increase the sensitivity of the EGFR-TKI-resistant H1975 cells to gefitinib (Figure 1SA). To verify the efficacy of BC in combination with gefitinib, we combined BC with gefitinib and evaluated the synergistic effect of the drug combination on H1975 cells, which are resistant to EGFR-TKIs. We found that the combination of gefitinib and BC (1:1) was superior to the use

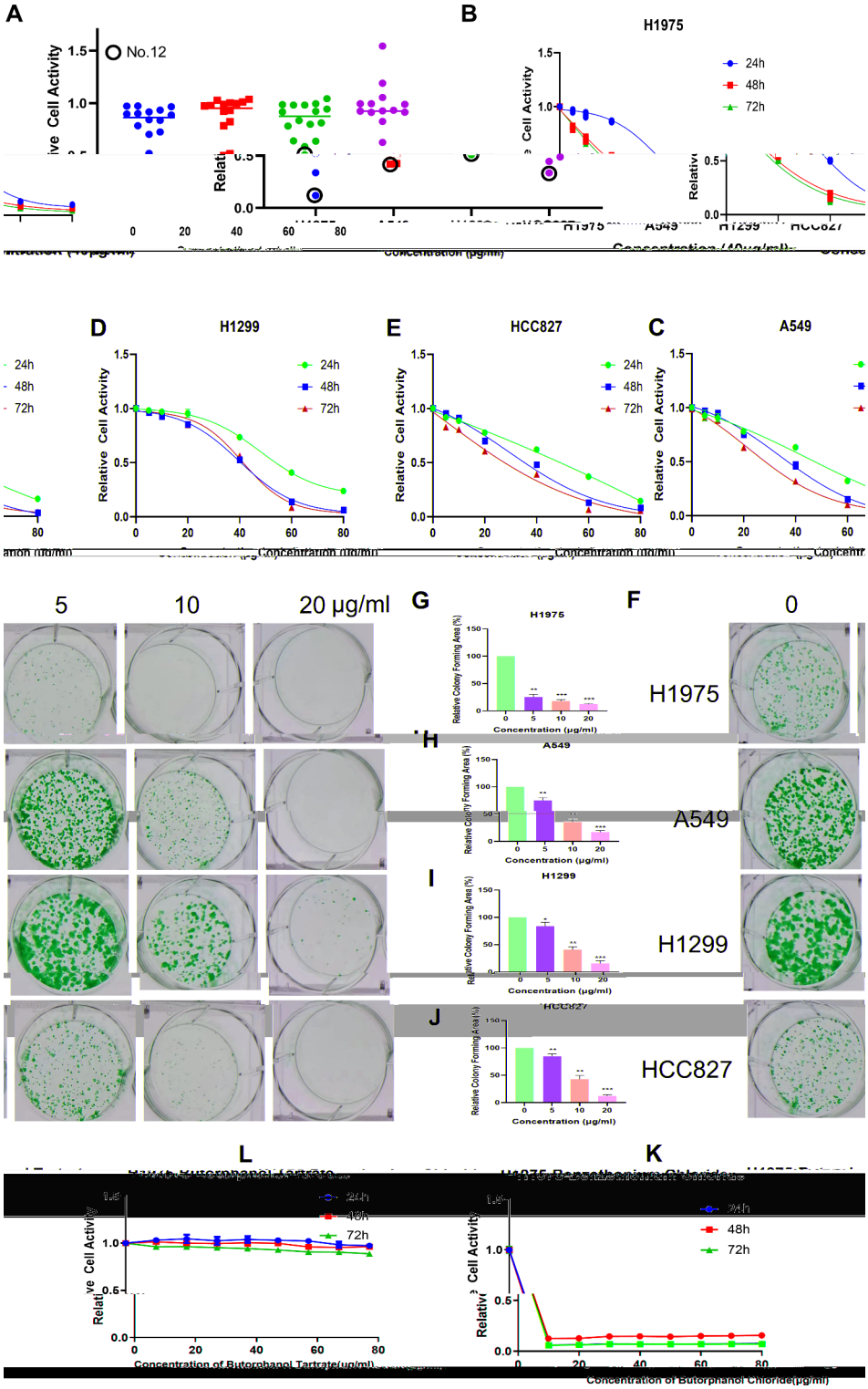

Fig. 1. Clinical anesthetics and analgesics inhibit cancer progression and alleviate resistance to EGFR-TKIs. (**A**) Effects of 16 analgesic anesthetic injections on the proliferation of H1975, A549, H1299, and HCC827 cells. (**B**, **C**, **D** and **E**) H1975, A549, H1299, and HCC827 cells were treated with increasing doses of butorphanol tartrate injection. (**F**, **G**, **H**, **I** and **J**) Effects of different concentrations of butorphanol tartrate injection on colony formation in the NSCLC cell lines H1975, A549, H1299, and HCC827. The area of colony formation was measured using ImageJ software. (**K**) Effects of butorphanol tartrate, a component of butorphanol tartrate injection, on H1975 cell proliferation. (**L**) Effects of benzethonium chloride, a component of butorphanol tartrate injection, on H1975 cell proliferation. The results are expressed as the mean ± standard deviation of three separate and distinct experiments (n = 3). (*P < 0.05, **P < 0.01, ***P < 0.001 compared with DMSO).

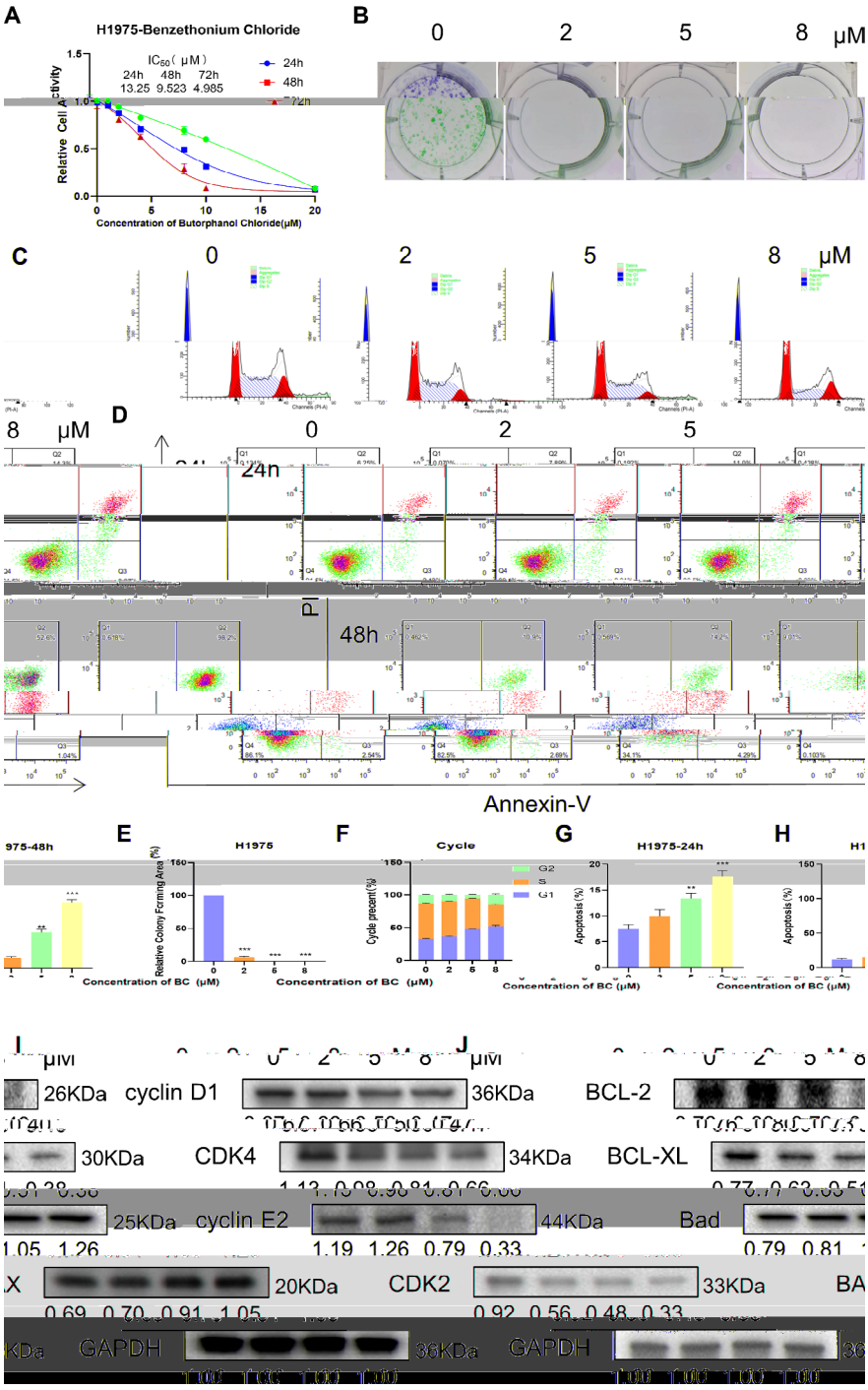

Fig. 2. Benzethonium chloride blocks the cell cycle and increases apoptosis. (**A**) H1975 cells were treated with increasing doses of benzethonium chloride (0–20 μM) for 24, 48, and 72 h and then cell viability was determined via a CCK8 assay and IC_{50} values were calculated. (**B** and **E**) Effects of different benzethonium chloride concentrations on H1975 colony formation in NSCLC cells. The area of colony formation was measured via ImageJ software. (**C** and **F**) H1975 cells were exposed to different concentrations of benzethonium chloride (0, 2, 5, or 8 μM) for 24 h and then the cell cycle was evaluated. (**D**, **G**, and **H**) H1975 cells were exposed to different concentrations of benzethonium chloride (0, 2, 5, or 8 μM) for 24 and 48 h followed by the detection of apoptotic cells. (I) Expression levels of apoptosis-related proteins after treatment of H1975 cells with different concentrations of benzethonium chloride (0, 2, 5, or 8 μM) for 24 h. GAPDH was used as an internal reference. (**J**) Expression levels of cell cycle-associated proteins after treatment of H1975 cells with different concentrations of benzethonium chloride (0, 2, 5, or 8 μM) for 24 h. GAPDH was used as an internal reference. The results are expressed as the mean ± standard deviation of three separate and distinct experiments (n = 3). (*P < 0.05, **P < 0.01, ***P < 0.001 compared with DMSO).

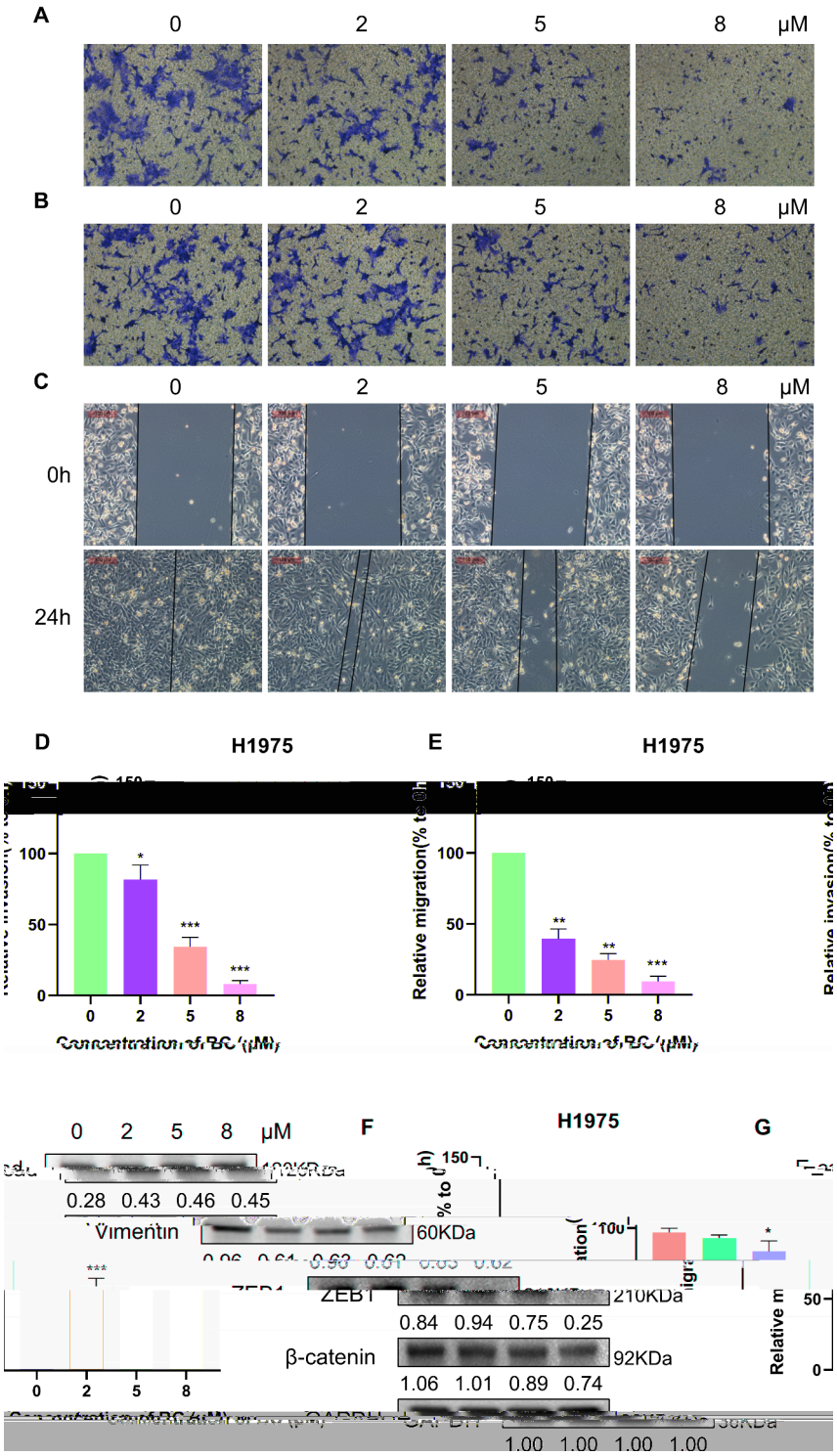

Fig. 3. Benzethonium chloride reduces cell migration and invasion. (**A** and **D**) Migration cell result maps were obtained via microscopic photography of H1975 cells treated with benzethonium chloride (0, 2, 5, or 8 μM) for 24 h. The results were analyzed via ImageJ. (**B** and **E**) Microscopic photographs of H1975 cells treated with benzethonium chloride (0, 2, 5, or 8 μM) for 24 h. The results were analyzed via ImageJ. (**C** and **F**) The width of the cell gap was determined via photographs of H1975 cells at 0 h and 24 h after treatment with benzethonium chloride (0, 2, 5, or 8 μM), respectively. The results were analyzed with ImageJ. (**G**) The expression levels of β-catenin, vimentin, ZEB1 and E-cad were analyzed by immunoblotting after H1975 cells were treated with different concentrations of benzethonium chloride (0, 2, 5, and 8 μM) for 24 h. GAPDH was used as an internal reference. The results are expressed as the mean ± standard deviation of three separate and distinct experiments (n = 3). (*P < 0.05, **P < 0.01, ***P < 0.001 compared with DMSO).

of either drug alone (Fig. 4A). To further investigate the enhancement of sensitivity of BC to gefitinib therapy, we fixed the concentration of gefitinib at 10 μM and applied a BC concentration gradient (ranging from 0 μM to 20 μM), for treatment durations of 24, 48, and 72 h. The results indicated that the combined effect of both compounds resulted in synergistic inhibition of cellular activity, which was observed to increase in a dose-dependent and time-dependent manner (Fig. 4B). Moreover, cotreatment with BC and gefitinib significantly downregulated the expression of cycle-associated proteins, such as CDK2, CDK4, cyclin D1, and cyclin E2, to induce the arrest of H1975 cells in the G1 phase of the cell cycle (Fig. 4C,D,G). Flow cytometry analysis revealed a significant increase in the level of apoptosis induced by 10 μM gefitinib when the cells were cotreated with BC (Fig. 4E,F). In addition, protein immunoblotting analysis revealed a dose-dependent increase in the expression of the proapoptotic proteins Bad and BAX and a decrease in the levels of the antiapoptotic proteins BCL-2 and BCL-XL in NSCLC cells upon treatment with BC and gefitinib (Fig. 4H).

BC inhibits gefitinib-promoted metastasis of EGFR-TKI-resistant cells

To explore the impact of combination treatments on the cellular metastasis of H1975 cells resistant to EGFR-TKIs, Transwell and wound healing experiments were performed. The results indicated that gefitinib at a concentration of 10 μM increased H1975 cell migration, whereas the combination of 2, 5, and 10 μM BC for 24 h significantly inhibited the migration of H1975 cells (Fig. 5A,D). To validate the effect of the drug combination on cell invasion, further results revealed that 10 μM gefitinib increased the invasive ability of H1975 cells and that BC inhibited the gefitinib-induced invasion of H1975 cells (Fig. 5B,E). Moreover, the effect of the combination of the two drugs was better than that of the single drugs in the wound healing experiment (Fig. 5C,F). The protein immunoblotting results revealed significant downregulation of the protein levels of β-catenin, vimentin, and ZEB1 and significant upregulation of E-cad (Fig. 5G).

BC regulated the P53 signaling pathway

To elucidate the molecular mechanism underlying the inhibitory effects of BC on the proliferation and metastasis of NSCLC, as well as its ability to alleviate resistance to EGFR-TKIs, we employed transcriptomic RNA sequencing (RNA-seq) in BC-treated H1975 cells. There were no significant changes in overall mRNA levels in the benzethonium chloride-treated H1975 cells (Figure 3SA). GSEA of H1975 cells treated with BC revealed significant differential enrichment of 56 KEGG signaling pathways, including those involved in DNA replication, the proteasome, the cell cycle, P53, and ferroptosis, all of which are related to tumor proliferation (Fig. 6A and Figure 3SB). Among these pathways, the DNA replication, cell cycle, small cell lung cancer, and cancer pathways were downregulated, whereas the cell adhesion signaling pathways were upregulated (Fig. 6C and Figure 3SC).

To further explore the molecular mechanisms underlying the inhibitory effects of BC on NSCLC proliferation and metastasis, we conducted differential expression analysis of the transcriptome of BC-treated cells ($|\log\text{FoldChange}| > 1$, P value < 0.05), and 831 genes were upregulated and 689 genes were downregulated in the cells of the BC-treated group relative to those of the untreated group (Figure 3SD). We performed KEGG pathway enrichment analysis of the significantly differentially expressed genes (DEGs). The downregulated genes were enriched mainly in the cell cycle, DNA replication and small cell lung cancer signaling pathways (Fig. 6B). The DEGs were associated with cell cycle signaling pathways, and the results revealed that most genes in the G1 phase of the cell cycle were downregulated and that the cyclin-dependent kinase inhibitor CDKN1 family proteins, which inhibit cyclin E2- and CDK2-binding genes, were upregulated (Fig. 6D,E). The results of fluorescence quantitative PCR after treating H1975 cells with gefitinib and BC in combination revealed that they promoted apoptosis and inhibited tumor growth, with increased expression of the Bad, BAX, P53, and TP53INP1 genes, and downregulated expression of the PARP1, BCL2, Caspase3, Caspase9, CCND1, CCNE2, CDK2, and CDK4 genes, which was largely consistent with the results of the previous heatmap of differential gene expression in the DNA replication and cell cycle signaling pathways (Fig. 6G and Figure 4S).

Transcriptomic analysis revealed that the cell cycle signaling pathway was the main downregulated pathway, with the P53 signaling pathway being located upstream of the cell cycle pathway. The CDKN1 family of proteins, regulated by the P53 signaling pathway, was upregulated, indicating that the molecular mechanism of BC's inhibitory effects on NSCLC proliferation and metastasis, as well as its ability to alleviate EGFR-TKI resistance, may be mediated through the P53 signaling pathway (Fig. 6E and Figure 3SE). Subsequent analysis of the transcriptome sequencing results revealed that TP53INP1 and the CDKN1 protein family were significantly upregulated in response to BC treatment, and these proteins were found to play a role in the inhibition of NSCLC proliferation and metastasis, as well as in the alleviation of EGFR-TKI resistance. These findings were further confirmed via protein immunoblotting (Fig. 6F).

BC inhibits and alleviates EGFR-TKI resistance in vivo

To demonstrate the in vivo effect, we employed an NSCLC xenograft tumor model. The present study investigated the in vivo efficacy of BC and gefitinib in inhibiting NSCLC growth in a nude mouse xenograft tumor model. The tumor volume data revealed that combined treatment with BC and gefitinib resulted in a more significant reduction in tumor growth than either drug alone (Fig. 7A,B). Additionally, the body weights of the mice remained stable throughout the treatment, indicating a high safety profile of BC in these mice (Fig. 7C). Histological staining clearly revealed extensive histopathological disturbances, such as swollen cells and necrosis, in the BC- and gefitinib-treated groups (Figure 5SA).

The results from protein immunoblotting and fluorescence quantification were in accordance with the findings from the in vitro studies, demonstrating that cotreatment with BC and gefitinib notably reduced the levels of cell cycle-associated proteins, increased the expression of apoptosis-related proteins, and inhibited the expression of EMT-related proteins and TP53INP1-related and CDKN1 proteins in vivo (Fig. 7D). Fluorescence

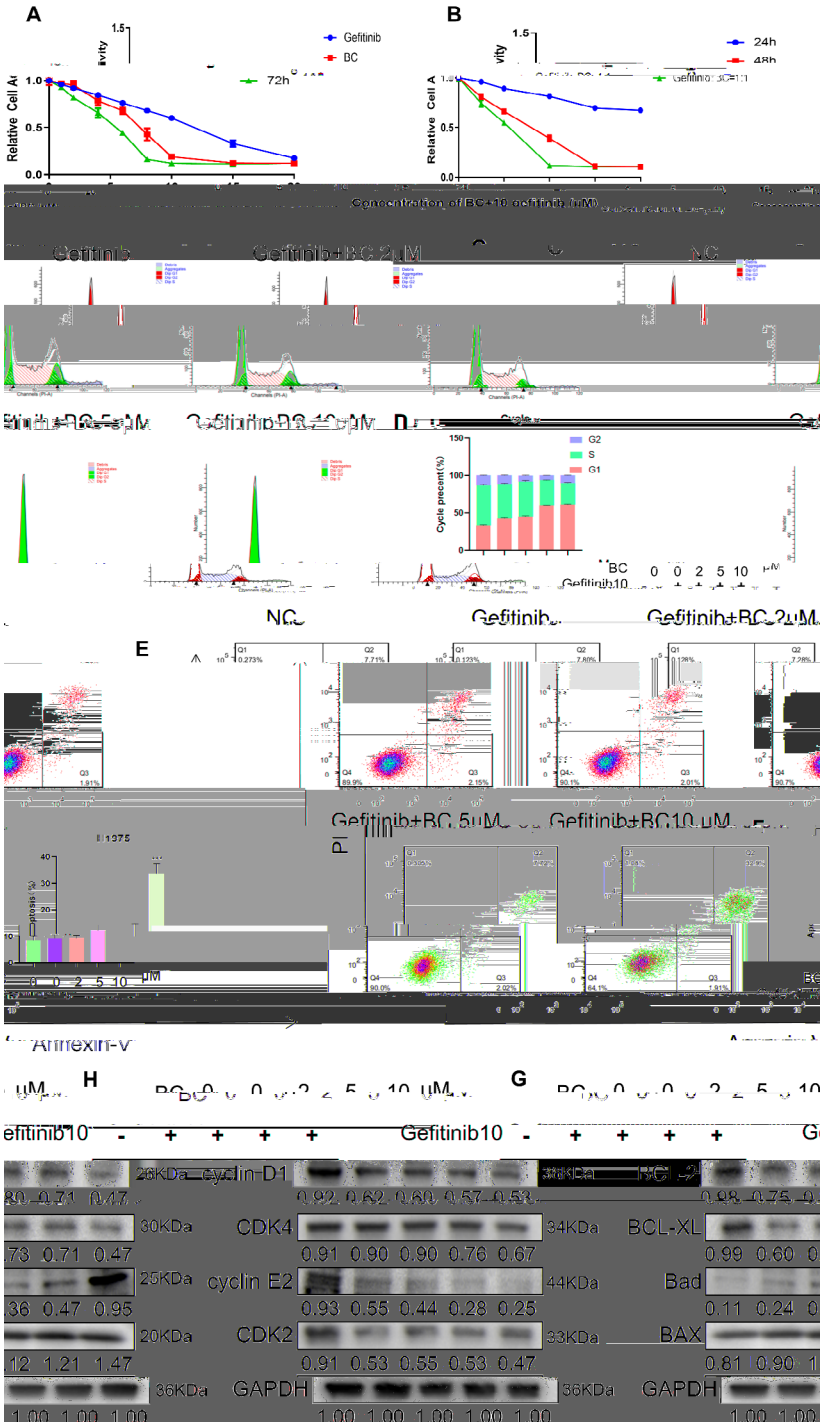

Fig. 4. Benzethonium chloride increases the ability of gefitinib to block the cell cycle and promote apoptosis in NSCLC. (**A**) H1975 cells were coadministered gefitinib and benzethonium chloride at a 1:1 ratio and cell viability was determined by a CCK8 assay after 24 h of treatment. (**B**) H1975 cells were treated with 10 μM gefitinib and benzethonium chloride (0, 1, 2, 4, 6, 8, 10, 15, or 20 μM) for 24, 48, or 72 h, and cell viability was determined via a CCK8 assay. (**C** and **D**) H1975 cells were treated with 10 μM gefitinib and benzethonium chloride (0, 2, 5, or 10 μM) for 24 h followed by analysis of the cell cycle. (**E** and **F**) H1975 cells were treated with 10 μM gefitinib and benzethonium chloride (0, 2, 5, or 10 μM) for 24 h followed by detection of apoptotic cells. (**G**) Expression levels of apoptosis-related proteins after treatment of H1975 cells with different concentrations of benzethonium chloride (0, 2, 5, or 10 μM) and 10 μM gefitinib for 24 h. GAPDH was used as an internal reference. (**H**) Expression levels of cycle-associated proteins after treatment of H1975 cells with different concentrations of benzethonium chloride (0, 2, 5, or 10 μM) and 10 μM gefitinib for 24 h. GAPDH was used as an internal reference. The results are expressed as mean ± standard deviation of three separate and distinct experiments (n = 3). (*P < 0.05, **P < 0.01, ***P < 0.001 compared with DMSO).

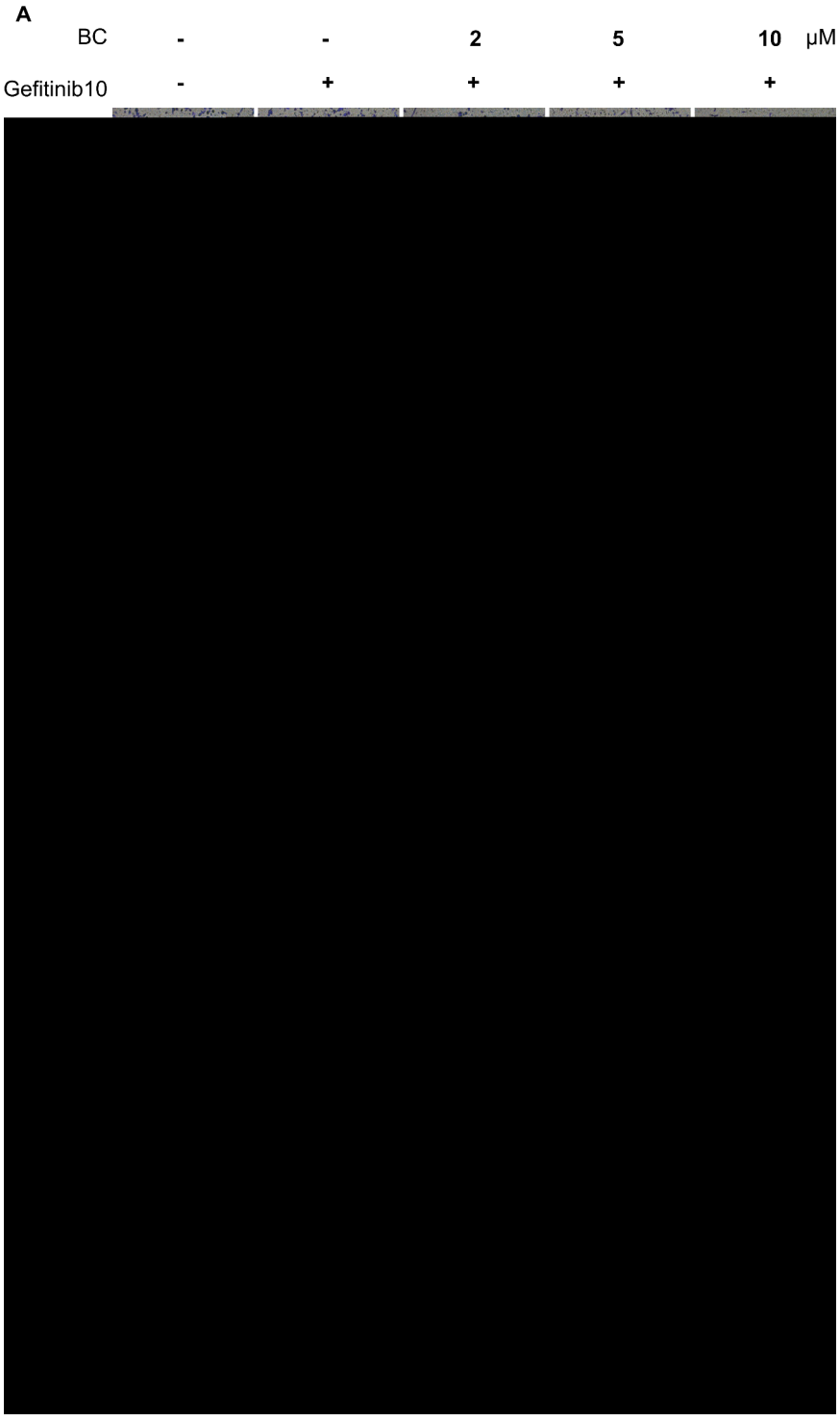

Fig. 5. Benzethonium chloride enhances the ability of gefitinib to inhibit cell migration and invasion in NSCLC. (**A**, **D**) Migration maps were obtained via microscopy after cotreatment of H1975 cells with 10 μM gefitinib and benzethonium chloride (0, 2, 5, or 10 μM) for 24 h. The results were analyzed via ImageJ. (**B**, **E**) The images of invasive cells were obtained via microscopic photography after cotreatment of H1975 cells with 10 μM gefitinib and benzethonium chloride (0, 2, 5, or 10 μM) for 24 h. The results were analyzed via ImageJ. (**C**, **F**) Gefitinib at 10 μM and benzethonium chloride (0, 2, 5, or 10 μM) were administered to H1975 cells, and the width of the cell gap was measured by imaging at 0 h and 24 h, respectively. (**G**) Expression levels of EMT-related proteins after treatment of H1975 cells with different concentrations of benzethonium chloride (0, 2, 5, or 10 μM) and 10 μM gefitinib for 24 h. GAPDH was used as an internal reference.

Figure 6

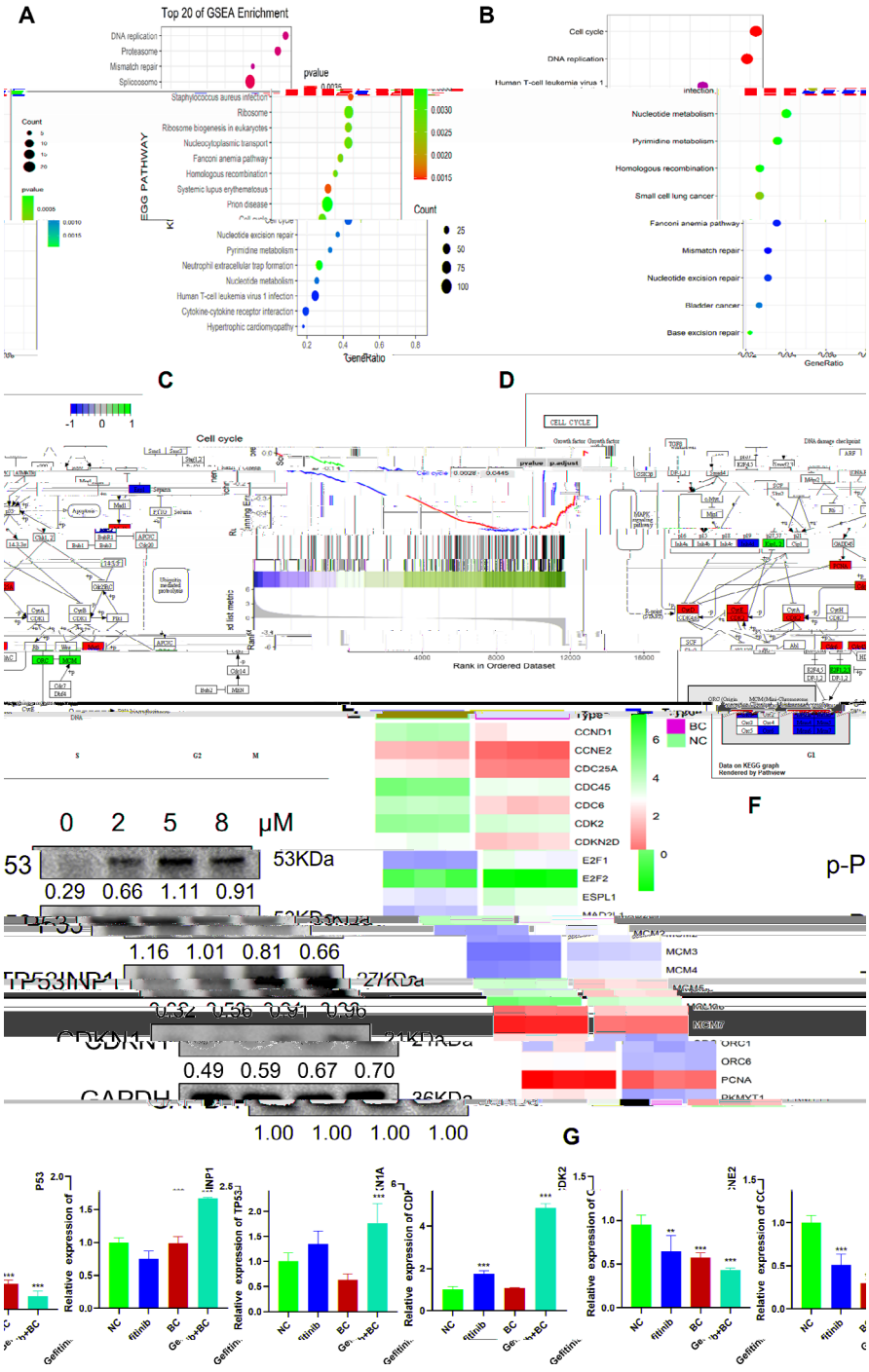

Fig. 6. Mechanism of action of benzethonium chloride against NSCLC. (**A**) Transcriptome GSEA of benzethonium chloride-treated H1975 NSCLC cells. (**B**) Enrichment of major signaling pathways associated with downregulated genes. (**C**) Enrichment of tumor-associated signaling pathways in benzethonium chloride-treated NSCLC H1975 cells. (**D**) Differential expression of genes involved in cell cycle signaling pathways (upregulated genes in red, downregulated genes in green). The pathway maps utilized information from the KEGG Pathway Database[12]. (**E**) Heatmap of differential gene expression related to cell cycle signaling pathways. (**F**) Expression levels of p-P53, P53, TP53INP1 and CDKN1 after treatment of H1975 cells with different concentrations of benzethonium chloride (0, 2, 5, or 8 μM) for 24 h. GAPDH was used as an internal reference. (**G**) mRNA levels of CDK2, CCNE2, P53, TP53INP1, and CDKN1A in H1975 cells treated with 10 μM benzethonium chloride and 10 μM gefitinib. The data were normalized to GAPDH to obtain the relative values. The results are expressed as mean ± standard deviation (n = 3). (*P < 0.05, **P < 0.01, ***P < 0.001 compared with DMSO).

Fig. 7. In vivo animal experiments verified that gefitinib and benzethonium chloride synergistically inhibited NSCLC progression. (**A** and **B**) Changes in tumor volume in mice treated with benzethonium chloride (20 mg/kg, negative control group given equal amounts of DMSO) and/or gefitinib (20 mg/kg, negative control group given equal amounts of DMSO) in the NSCLC xenograft tumor model. (**C**) Daily body weights of the mice. (**D**) Immunoblotting analysis of cycle-associated proteins, apoptosis-related proteins, EMT-related proteins and P53-related proteins after treatment of the NSCLC xenograft tumor model, using GAPDH as an internal reference. (**E**) Immunohistochemistry was performed to detect P53, TP53INP1, CDK2, cyclin E2, and CDKN1 levels.

quantification revealed that the expression of TP53INP1, P53 and CDKN1 family genes was upregulated (Figure 5SB). Immunohistochemical results revealed that the expression of the antiapoptotic proteins BCL-2 and BCL-XL was downregulated, whereas the protein levels of P53, TP53INP1 and CDKN1 were upregulated (Fig. 7E and Figure 5SA). Moreover, the levels of the cell cycle-associated proteins CDK2, CDK4, cyclin D1, and cyclin E2 were downregulated after cotreatment with BC and gefitinib (Fig. 7E and Figure 5SA). Moreover, we found that both BC and BC combined with gefitinib significantly decreased the expression of cell cycle-associated proteins and upregulated the expression of TP53INP1 and P53-regulated cyclin-dependent kinase inhibitor CDKN1 family proteins in vivo. In vivo, we demonstrated that benzethonium chloride could modulate the P53 signaling pathway to inhibit the cell cycle regulation of non-small cell lung cancer proliferation and metastasis and enhance its sensitivity to EGFR-TKI therapy.

Discussion

The number of cancer patients is increasing annually, the number of patients experiencing cancer pain is also significantly increasing, and the treatment of cancer pain is receiving increasing attention as an important part of oncology treatment. Uncontrolled pain can lead to physical and psychological suffering[16] and can seriously affect the quality of life of patients[17]. The presence and severity of pain may influence the outcome of clinical treatment[18,19]. The experience of pain can positively or negatively affect patient outcomes[20]. Increasing the frequency and quality of patient pain management can improve compliance with anti-neoplastic therapy[21]. Therefore, effective pain management is crucial.

In this study, we screened 16 commonly used anesthesia analgesic injections and found that butorphanol tartrate injection effectively inhibited the proliferation of NSCLC cells (Fig. 1A). Butorphanol tartrate injection is an analgesic with mixed agonist antagonist activity at opioid receptors. Receptor specificity has been used to limit respiratory depression and gastrointestinal side effects and reduce the risk of dependence, theoretically offering advantages over traditional opioids such as morphine and pethidine in the treatment of moderate as well as severe pain, and butorphanol has been used as a preoperative sedative and analgesic for cancer pain[22]. In addition, butorphanol has been noted to have an antitumor effect on ovarian cancer[23] and it reverses multidrug resistance in leukemia cells[24], but the mechanism of action remains unclear.

The morbidity and mortality of lung cancer are at the forefront of cancer incidence and death, and non-small cell lung cancer is the main type. The overexpression or mutation of the epidermal growth factor receptor (EGFR) is a major cause of NSCLC development and progression[25]. Gefitinib, a tyrosine kinase inhibitor (TKI), has been shown to significantly improve patient survival and is widely used as a first-line treatment for patients with EGFR-mutated advanced NSCLC[25]. Unfortunately, most patients inevitably relapse due to drug resistance[26]. The results of this study revealed that the analgesic butorphanol tartrate exhibited antitumor activity in NSCLC cell lines (Fig. 1A,B). We found that the main antitumor component of butorphanol tartrate injection is BC. BC has been found to have anticancer effects in head and neck squamous cell carcinoma (HNSCC), pharyngeal squamous carcinoma, hepatocellular carcinoma and NSCLC[26–29]. Proteomic studies have shown that BC can induce NSCLC cell cycle arrest by promoting the degradation of cyclin D1[29]. In this study, we found through transcriptome studies that BC can significantly inhibit the transcription of genes related to multiple signaling pathways, such as the cell cycle and DNA replication (Fig. 6 and Figure 3S). The P53 pathway is known to trigger several important biological processes, such as cell cycle arrest, apoptosis, DNA repair, replicative senescence, and differentiation, through the transcriptional activation of several genes. TP53INP1, a target gene of P53, induces cell growth arrest and apoptosis by regulating P53 transcriptional activity[27]. TP53INP1 physically interacts with P53 and is a major player in the P53-driven oxidative stress response. In early pancreatic carcinogenesis, TP53INP1 is downregulated, but its restoration has been shown to inhibit pancreatic tumor development[28]. The overexpression of these isoforms induces G1 phase arrest and increases P53-mediated apoptosis[29]. Transcriptome, real-time PCR and western blotting analyses revealed that benzethonium chloride treatment significantly inhibited the transcription of genes related to the G1 phase of the cell cycle (Figs. 2C,I and 6G). Moreover, the TP53INP1 and CDKN1 proteins were upregulated, suggesting that the molecular mechanism of the inhibitory effect of benzethonium chloride on the proliferation of NSCLC, as well as the reduction in EGFR-TKI resistance, may be mediated through the P53 signaling pathway. These results suggest that benzethonium chloride inhibits lung cancer metastasis by increasing the function of p53 through the complex action of P53 and TP53INP1.

Conclusion

Among the 16 anesthetic and analgesic injections commonly used in the clinic, butorphanol tartrate injection effectively inhibited the proliferation of NSCLC cells and alleviated gefitinib resistance. Benzethonium chloride, the main component of butorphanol tartrate injection, inhibits tumor progression and enhances the sensitivity of EGFR-TKI-resistant cells to gefitinib therapy in NSCLC by upregulating the P53 signaling pathway to affect EMT, the cell cycle and apoptosis via multiple signaling pathways (Fig. 8).

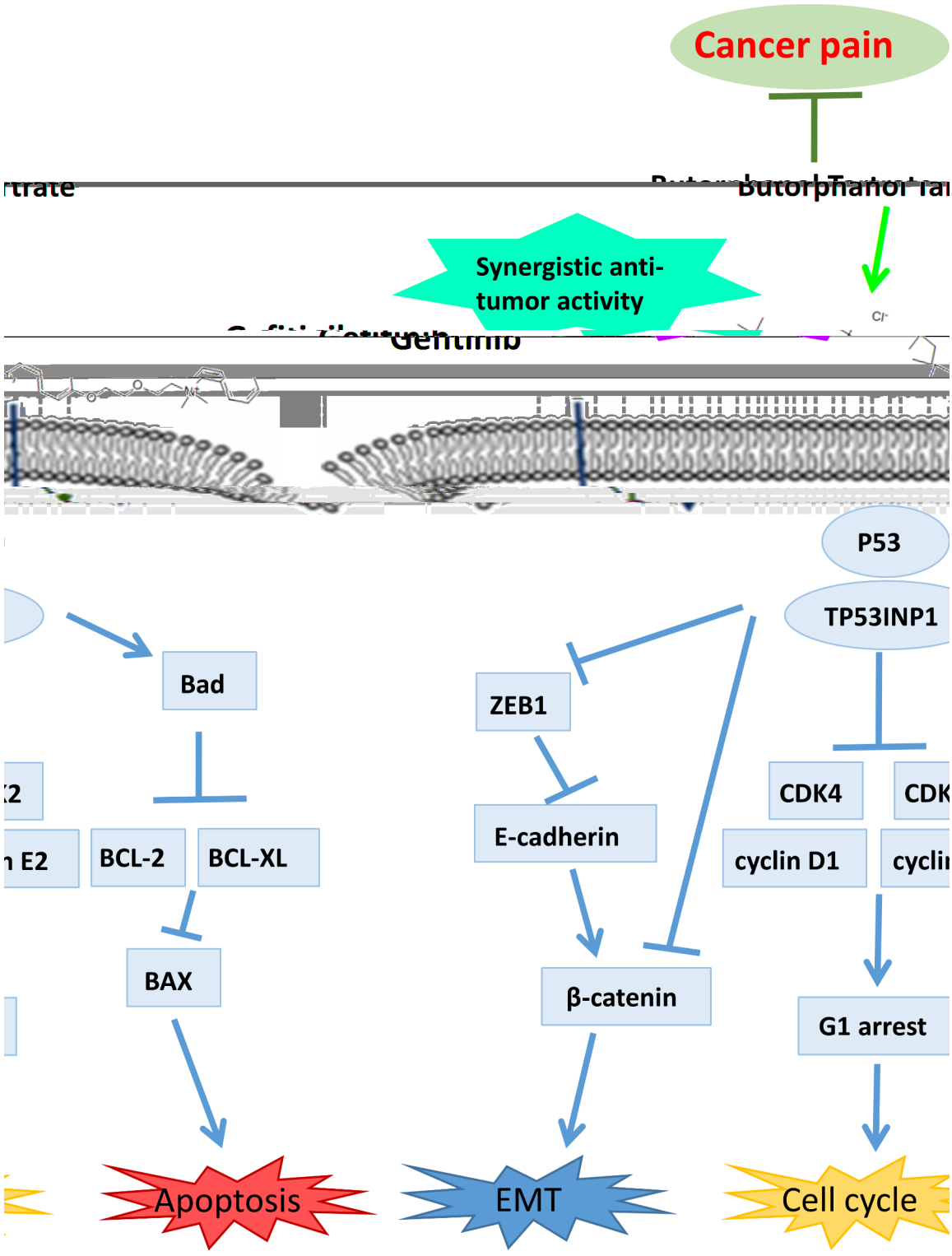

Fig. 8. Potential antitumor mechanism of the main component of butorphanol tartrate injection (benzethonium chloride).

Data availability

The datasets used in this study are available from the corresponding author upon reasonable request.

Received: 12 August 2024; Accepted: 29 November 2024
Published online: 04 December 2024

References

1. Siegel, R. L. et al. Cancer statistics, 2021. *CA Cancer J. Clin.* **71**(1), 7–33 (2021).
2. Martinez, K. A. et al. Decision regret following treatment for localized breast cancer: Is regret stable over time?. *Med. Decis. Making* **35**(4), 446–457 (2015).
3. Dubowitz, J. A., Sloan, E. K. & Riedel, B. J. Implicating anaesthesia and the perioperative period in cancer recurrence and metastasis. *Clin. Exp. Metastasis* **35**(4), 347–358 (2018).
4. Midha, A., Dearden, S. & McCormack, R. EGFR mutation incidence in non-small-cell lung cancer of adenocarcinoma histology: A systematic review and global map by ethnicity (mutMapII). *Am. J. Cancer Res.* **5**(9), 2892–2911 (2015).
5. Rosell, R. et al. Erlotinib versus standard chemotherapy as first-line treatment for European patients with advanced EGFR mutation-positive non-small-cell lung cancer (EURTAC): A multicentre, open-label, randomised phase 3 trial. *Lancet Oncol.* **13**(3), 239–246 (2012).
6. Park, S. et al. Resistance mechanisms of EGFR tyrosine kinase inhibitors, in EGFR exon 20 insertion-mutant lung cancer. *Eur. J. Cancer* **208**, 114206 (2024).
7. Ardeshir-Larijani, F. & Ramalingam, S. S. The MARIPOSA trials - implications for the treatment of EGFR-mutant NSCLC. *Nat. Rev. Clin. Oncol.,* (2024).
8. Morgillo, F. et al. Mechanisms of resistance to EGFR-targeted drugs: Lung cancer. *ESMO Open* **1**(3), e000060 (2016).
9. Yu, H. A. et al. Acquired Resistance of EGFR-Mutant Lung Cancer to a T790M-Specific EGFR Inhibitor: Emergence of a Third Mutation (C797S) in the EGFR Tyrosine Kinase Domain. *JAMA Oncol.* **1**(7), 982–984 (2015).
10. Tsimberidou, A. M. et al. Molecular tumour boards - current and future considerations for precision oncology. *Nat. Rev. Clin. Oncol.* **20**(12), 843–863 (2023).
11. Bendixen, M. et al. Postoperative pain and quality of life after lobectomy via video-assisted thoracoscopic surgery or anterolateral thoracotomy for early stage lung cancer: A randomised controlled trial. *Lancet Oncol.* **17**(6), 836–844 (2016).
12. Kanehisa, M., Furumichi, M., Sato, Y., Kawashima, M. & Ishiguro-Watanabe, M. KEGG for taxonomy-based analysis of pathways and genomes. *Nucleic Acids Res.* **51**, D587–D592 (2023).
13. Kanehisa, M. & Goto, S. KEGG: Kyoto encyclopedia of genes and genomes. *Nucleic Acids Res.* **28**, 27–30 (2000).
14. Kanehisa, M. Toward understanding the origin and evolution of cellular organisms. *Protein Sci.* **28**, 1947–1951 (2019).
15. Tan, W. C. C. et al. Overview of multiplex immunohistochemistry/immunofluorescence techniques in the era of cancer immunotherapy. *Cancer Commun. (Lond)* **40**(4), 135–153 (2020).
16. van den Beuken-van Everdingen, M. H. et al. Update on prevalence of pain in patients with cancer: Systematic review and meta-analysis. *J. Pain Symptom. Manage* **51**(6), 1070-1090.e9 (2016).
17. Green, C. R., Hart-Johnson, T. & Loeffler, D. R. Cancer-related chronic pain: Examining quality of life in diverse cancer survivors. *Cancer* **117**(9), 1994–2003 (2011).
18. Quinten, C. et al. Baseline quality of life as a prognostic indicator of survival: A meta-analysis of individual patient data from EORTC clinical trials. *Lancet Oncol.* **10**(9), 865–871 (2009).
19. Efficace, F. et al. Is a patient's self-reported health-related quality of life a prognostic factor for survival in non-small-cell lung cancer patients? A multivariate analysis of prognostic factors of EORTC study 08975. *Ann. Oncol.* **17**(11), 1698–1704 (2006).
20. Beck, S. L. et al. Core aspects of satisfaction with pain management: Cancer patients' perspectives. *J. Pain Symptom Manage* **39**(1), 100–115 (2010).
21. Basch, E. et al. Symptom monitoring with patient-reported outcomes during routine cancer treatment: A randomized controlled trial. *J. Clin. Oncol.* **34**(6), 557–565 (2016).
22. Vogelsang, J. & Hayes, S. R. Butorphanol tartrate (stadol): A review. *J. Post Anesth. Nurs.* **6**(2), 129–135 (1991).
23. Wang, B. et al. Butorphanol inhibits the malignant biological behaviors of ovarian cancer cells via down-regulating the expression of TMEFF1. *Onco. Targets Ther.* **13**, 10973–10981 (2020).
24. Wen, J. et al. Butorphanol, a synthetic opioid, sensitizes ABCB1-mediated multidrug resistance via inhibition of the efflux function of ABCB1 in leukemia cells. *Oncol. Rep.* **34**(2), 755–762 (2015).
25. Gelatti, A. C. Z., Drilon, A. & Santini, F. C. Optimizing the sequencing of tyrosine kinase inhibitors (TKIs) in epidermal growth factor receptor (EGFR) mutation-positive non-small cell lung cancer (NSCLC). *Lung Cancer* **137**, 113–122 (2019).
26. Zhang, T. et al. Discovery of a novel third-generation EGFR inhibitor and identification of a potential combination strategy to overcome resistance. *Mol. Cancer* **19**(1), 90 (2020).
27. Saadi, H., Seillier, M. & Carrier, A. The stress protein TP53INP1 plays a tumor suppressive role by regulating metabolic homeostasis. *Biochimie* **118**, 44–50 (2015).
28. Seux, M. et al. TP53INP1 decreases pancreatic cancer cell migration by regulating SPARC expression. *Oncogene* **30**(27), 3049–3061 (2011).
29. Tomasini, R. et al. TP53INP1s and homeodomain-interacting protein kinase-2 (HIPK2) are partners in regulating p53 activity. *J. Biol. Chem.* **278**(39), 37722–37729 (2003).

Acknowledgements

The authors would like to thank Novogene Biotechnology Company for their help with RNA-seq.

Author contributions

M.Q.L., H.L.T., L.L., H.L.L., X.P.Z., T.T.M. and S.M.Z. designed this research and wrote the manuscript. H.L.T., X.P.Z., T.T.M., and J.L.C. articipated in various experimental parts of the implementation of the project, discussed the results, and revised the manuscript. Y.Q.Z. and J.L.C. revised the manuscript. H.L.T., L.L. and H.L.L. contributed equally to this work. All of the authors reviewed and approved the final manuscript.

Funding

National Natural Science Foundation of China (Grant No: 82074093), Medical Science and Technology Project of Zhejiang Province (Grant No: 2023RC140), Zhejiang Traditional Chinese Medicine Administration (Grant No: 2021AX002), State Administration of Traditional Chinese Medicine Science and Technology Department-Zhejiang Provincial Administration of Traditional Chinese Medicine Co-construction of Key Laboratory of Research on Prevention and Treatment for depression syndrome (Grant No: GZY-ZJ-SY-2402).

Declarations

Competing interests

The authors declare that they have no competing interests.

Ethical approval and consent to participate

All animal experiments were approved by the Animal Ethics Committee of the Zhejiang Academy of Traditional Chinese Medicine and were conducted according to the Guidelines for the Care and Use of Animals for Scientific Research.

Consent for publication

The authors declare that they have no competing financial interests or personal relationships that could have appeared to influence the work reported in this paper.

Additional information

Supplementary Information The online version contains supplementary material available at https://doi.org/10.1038/s41598-024-81912-y.

Correspondence and requests for materials should be addressed to S.Z. or M.L.

Reprints and permissions information is available at www.nature.com/reprints.

Publisher's note Springer Nature remains neutral with regard to jurisdictional claims in published maps and institutional affiliations.